Unveiling the Anti-Radical Potential of Galangin — A Detailed Density Functional Theory Investigation

Maciej Spiegel

Department of Organic Chemistry and Pharmaceutical Technology, Faculty of Pharmacy, Wroclaw Medical University, Borowska 211A, 50-556 Wroclaw, Poland

KEYWORDS: galangin, antiradical activity, quantum mechanics, flavonoid, molecular interactions, hydroperoxyl radical, electronic structure, thermodynamics, kinetics, antioxidant research

ABSTRACT: A comprehensive quantum mechanical investigation into the antiradical activity of galangin (**Glg**), a natural flavonoid recognized for its robust antioxidant and anti-inflammatory properties, is presented. The compound undergoes successive deprotonation at C_7 (pK_a=7.48), C_3 (pK_a=9.34), and C_5 (pK_a=12.07). At pH 7.4, the predominant species are the neutral form (54.37%) and the first deprotonation product (45.11%), with the dianion present at a minor level (0.51%). According to eH-DAMA results, **Glg** exhibits improved antiradical effectiveness in water compared to apolar solvents. In both solvents, exergonic pathways towards $^{\bullet}$OOH radicals involve radical adduct formation at C_2, while the highest propensity for HAT is associated with the C_3 hydroxyl. Electron transfer pathways are not preferred, as indicated by Marcus's parabola. The overall reaction rate was established at 3.77×10^3 M^{-1} s^{-1} in pentyl ethanoate and 1.69×10^5 M^{-1} s^{-1} in water, considering the molar fractions of individual species and hydroperoxyl radicals at pH=7.4. The magnitude of the same reaction rate within the physiological pH range (pH=1.5 – 8.5) is consistently not less than 3.5, gradually reaching a peak value of 5.48 starting from pH=5. Furthermore, all **Glg** species readily undergo regeneration mediated by $O_2^{\bullet-}$.

INTRODUCTION

Oxidative stress is a physiological condition characterized by an imbalance between the production of reactive oxygen species (ROS) and cellular antioxidant defence mechanisms. ROS, including free radicals and other oxygen-derived molecules, are integral to normal cellular metabolism and play a crucial role in signalling pathways.[1,2] However, environmental factors or certain pathological conditions can lead to their excessive production, causing cellular damage and dysfunction.[3] The disruption of redox homeostasis has been implicated in various diseases, including neurodegenerative disorders[4,5], cardiovascular diseases[6], and cancer[7]. Understanding the molecular mechanisms underlying oxidative stress is crucial for developing therapeutic interventions to mitigate its adverse effects on cellular function.

Antioxidants, a diverse group of molecules, counteract the harmful effects of oxidative stress by neutralizing and scavenging reactive oxygen species. These compounds, which include vitamins (e.g., vitamin C and E)[8], minerals (e.g., selenium)[8], and phytochemicals (e.g., flavonoids and polyphenols)[9], act through mechanisms such as donating electrons or hydrogen atoms to stabilize free radicals.[10,11] Antioxidants play a pivotal role in maintaining cellular redox balance and protecting biomolecules, such as lipids, proteins, and nucleic acids, from oxidative damage.[1,2] Numerous studies[12] have highlighted the potential health benefits of a diet rich in antioxidants, emphasizing their role in preventing or ameliorating oxidative stress-related diseases.

Galangin (denoted as **Glg** and depicted in **Scheme 1**) is a natural flavonoid found in various plant sources, including *Alpinia officinarum* and *Helichrysum aureonitens*, and propolis.[13] This bioactive polyphenol has attracted scientific interest due to its potent antioxidant and anti-inflammatory properties. Research have indicated that **Glg** exhibits protective effects against oxidative stress-induced cellular damage by modulating intracellular signalling pathways and enhancing the activity of endogenous antioxidant enzymes. Moreover, galangin has shown promise in diverse therapeutic applications, ranging from neuroprotection to anti-cancer effects.[14–17] The exploration of galangin's molecular mechanisms and its potential role in mitigating oxidative stress-related disorders underscores its significance in the ongoing pursuit of novel and effective therapeutic agents.

Computational studies on antioxidants have become increasingly instrumental in elucidating the intricate molecular mechanisms underlying their efficacy. Utilizing advanced computational tools, such as quantum chemical calculations, researchers can explore the interactions between antioxidants and reactive oxygen species at the atomic level. These simulations provide valuable insights into the thermodynamics and kinetics of antioxidant reactions, aiding in the identification of key structural features that enhance their scavenging capabilities.[10,11,18] Furthermore, computational approaches contribute to the rational design of novel antioxidant compounds with optimized properties, guiding the development of potential therapeutic agents.[19–21] By bridging the gap between experimental findings and theoretical predictions, computational studies on antioxidants enhance our understanding of their complex behaviour in biological systems, offering a valuable platform for advancing antioxidant research and drug discovery.

In this research paper, the focus is on employing quantum mechanics to investigate the anti-radical activity of **Glg**. Drawing from the already conducted research it can be postulated that the substance,

owing to its recognized antioxidant properties, will demonstrate a capacity to efficiently neutralize and scavenge reactive radical species, thereby mitigating oxidative stress. The computational framework enables an in-depth exploration of the molecular interactions, structural determinants, and electronic features governing this efficacy. This research aims to contribute nuanced insights to the realm of antioxidant studies, with the potential to inform the development of novel therapeutic agents grounded in the molecular attributes of galangin.

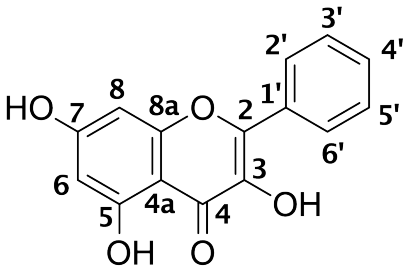

Scheme 1. Molecular structure of galangin (**Glg**) with site numbering.

COMPUTATIONAL DETAILS

The low-energy ground-state conformer of neutral galangin was systematically generated using a robust conformer search procedure that combines metadynamic sampling and z-matrix genetic crossing, specifically the iMTD-GC method implemented in the CREST driver program.[22]

Electronic structure calculations in this study were conducted using the Gaussian 16 (rev. C.01) software package.[23] For geometry optimizations and frequency calculations, the density functional theory (DFT) approach was employed, specifically utilizing the M05-2X/6-311+G(d,p) level of theory. The M05-2X functional was selected for its proficiency in addressing noncovalent interactions, kinetics, and thermochemistry. Its reliability is supported by extensive validation against barrier heights, conformational energy, and bond dissociation energies.[24] Moreover, M05-2X has demonstrated efficacy in modelling open-shell systems, particularly estimating energies associated with reactions involving free radicals.[25] It also stand out as one of the top-performing DFT approximations, alongside LC-xPBE, M06-2X, BMK, B2PLYP, and MN12SX, based on a benchmark study assessing rate constant calculations for radical molecule reactions in aqueous solutions.[26]

Solvation effects were incorporated into the study using the universal solvation model based on solute electron density (SMD)[27] with pentyl ethanoate (ε=4.73[28]) and water (ε=78.35[28]) chosen to reproduce physiological conditions of cellular environments. The choice of SMD was grounded in its demonstrated suitability for simulating solvents with varied characteristics and media, whether charged or non-charged.[27] Notably, SMD has proven effective in mixed models and has been successfully applied for geometry optimization and vibrational calculations in solution settings. Empirical validation for a wide range of solutes and liquid environments further supports its appropriateness.[29]

Unrestricted calculations were specifically implemented for open-shell systems in this study. To ensure result accuracy for radical species, thorough checks for spin contamination were conducted. In all instances, deviations from the ideal value were negligible following the annihilation of the initial spin contamination. The identification of local minima relied on the absence of imaginary frequencies, while transition states were discerned through the presence of a single frequency precisely corresponding to the anticipated motion along the reaction coordinate. Additionally, the accuracy of the identified structures was confirmed through Intrinsic Reaction Coordinate (IRC) computations[30,31] providing assurance that the calculated transition states appropriately linked with the reactants and products of the intended reaction, reinforcing the reliability of the theoretical predictions.

Acid-Base Equilibria

To ascertain acid constants for the substances under investigation, a parameter-fitted approach was employed as outlined by reference.[32] This method involves computing pK_a values utilizing a linear fitting expression:

$$\mathrm{p}K_a = m\Delta G_{BA} + C_0$$

Here, ΔG_{BA} represents the Gibbs free energy difference between the conjugated base and the corresponding acid. The parameters m and C_0 are variable and contingent upon the specific substituents and the computational level employed. Only acid-base species with molar fractions ($^M f$) exceeding 0.1% were considered for inclusion in the study.

Thermochemistry

The assessment of the thermodynamic feasibility of various processes involved analysing the Gibbs free energies of reaction. The energies of solvated electron and proton were sourced from the study by Marković et al.[33]

Relative energies, incorporating thermodynamic corrections at 298.15 K, were calculated with respect to the sum of the isolated reactants, all referenced to the 1 M standard state. Additionally, solvent cage effects, accounting for entropy loss due to liquid-phase effects, were taken into consideration. This correction, following the approach proposed by Okuno[34], integrated the free volume theory[35]. For a bimolecular reaction leading to a single product, the application of this correction at 298 K resulted in a reduction of 2.55 kcal mol^{-1} in the Gibbs free energy in solution compared to the same reaction in the gas phase. Neglecting both the standard state and solvent effects simultaneously in the calculation of reaction barriers would result in a substantial underestimation of rate constants, approximately by a factor of 1800, for bimolecular reactions at room temperature.[36] This highlights the significant influence of solvent effects on both the thermodynamics and kinetics of reactions in the solution phase

Kinetics

Kinetic data were obtained using the QM-ORSA protocol, a validated method designed for calculating rate constants in solution, demonstrating uncertainties comparable to experimental measurements [11,18,36] Detailed information on the computational procedures can be found in the respective references.

The conventional Transition State Theory (TST)[37–39] was employed for rate constant calculations, utilizing harmonic vibrational

frequencies and non-symmetrical, unidimensional Eckart tunnelling corrections.[40] The TST rate constant (k^{TST}) is expressed as:

$$k^{TST} = \sigma\kappa(T)\frac{k_b T}{h}e^{-\left(\frac{\Delta G^{\neq}}{RT}\right)}$$

Here, $\Delta G^{\neq}$ represents the Gibbs activation energy, σ is the reaction path degeneracy[41,42], $\kappa(T)$ is the tunneling correction[43], T is the temperature, and k_b, h and R are the Boltzmann, Planck, and ideal gas constants, respectively. σ signifies the number of equivalent reaction paths, and for the studied reactions, $\sigma = 1$ due to the absence of rotational symmetry in the transition state geometries.[37,39,44]

For Single Electron Transfer (SET) reactions, activation energies were determined using Marcus theory.[45] The formula for calculating $\Delta G^{\neq}$ is given by:

$$\Delta G^{\neq} = \frac{\lambda}{4}\left(1 + \frac{\Delta G_{SET}}{\lambda}\right)^2$$

Here, ΔG_{SET} represents the free energy of the reaction, and λ corresponds to the reorganization energy. In cases of vertical electron transfer within a reactant complex, ΔG_{SET} values were computed between the reactant and product complexes. Additionally, λ values were determined as the sum of internal (λ_i) and solvent (λ_o) reorganization energies.[46]

As some rate constants of radical reactions tend to approach the diffusion limit, a correction using the Collins–Kimball theory[47] was applied. The corrected rate constant (k) is given by:

$$k = \frac{k_D k^{TST}}{k_D + k^{TST}}$$

Here, k^{TST} represents the thermal rate constant obtained from TST calculations, and k_D is the steady-state Smoluchowski rate constant for an irreversible bimolecular diffusion-controlled reaction[48].

The total rate coefficients for the reactions (k_{total}) were determined by summing the contributions from each reaction path (i):

$$k_{total} = \sum_{i}^{n} k_i$$

The overall rate coefficients ($k_{overall}$) were calculated by considering the molar fractions (^{M}f) of the acid–base species involved in each chemical route at the pH of interest.

$$k_{overall} = {}^{M}f \quad k_{total} + {}^{M}f^{-}k^{-}_{total} + {}^{M}f^{2-}k^{2-}_{total}$$

The molar fractions are computed from the pK_a values of the reactants:

$$^{m}f^{2-} = \frac{1}{1 + \beta_1[H^+] + \beta_2[H^+]^2}$$
$$^{m}f^{-} = \beta_1[H^+](^{m}f^{2-})$$
$$^{m}f = \beta_2[H^+]^2(^{m}f^{2-})$$

where

$$\beta_1 = 10^{\mathrm{p}K_{a2}}$$

$$\beta_2 = 10^{\mathrm{p}K_{a2}+\mathrm{p}K_{a1}}$$

The percent contributions of each reaction mechanism (Γ) are then estimated using the formula:

$$\Gamma_i = 100 \times \frac{k_i}{k_{total}}$$

This approach provides a quantitative breakdown of the contribution of each mechanism to the total reaction rate, facilitating a more detailed analysis of the reaction network.

RESULTS AND DISCUSSION

Acid-Base Equilibria

In aqueous solutions, the equilibrium between neutral and charged species in molecules with acid–base characteristics, governed by the pK_a-pH relationship, plays a crucial role. This equilibrium significantly influences the antioxidant behavior of the substances.[49]

Currently, no experimental pK_a values for **Glg** are available, necessitating reliance on the theoretical estimates presented in this paper. However, the proposed methodology [32] has been previously validated as reliable for polyphenolic compounds, producing results closely aligned with experimentally measured values.

The first dissociation constant corresponds to the deprotonation of the phenolic OH located at C_7 (pK_{a1}=7.48), followed by C_3 (pK_{a2}=9.34), and finally C_5 group (pK_{a3}=12.07). The hydroxyl group at C_7 exhibits the highest propensity for deprotonation, consistent with previous observations.[50–53] Additionally, the intramolecular hydrogen bonding with the carbonyl residue at C_4, involving the acidic hydrogens of C_3 and C_5 groups, stabilizes the system, reducing the tendency for dissociation[54]. Therefore, the proposed deprotonation pathway is deemed reasonable.

As indicated by the graph depicting molar fraction as a function of pH (**Figure 1**), the species with the largest population at pH=7.4 comprises the neutral form ($^{M}f = 54.37\%$) and the product of the first deprotonation ($^{M}f^{-} = 45.11\%$). Although the dianion is predicted to exist only to a minor extent under the same conditions, its population is not negligible ($^{M}f^{2-} = 0.51\%$) and should be duly considered.

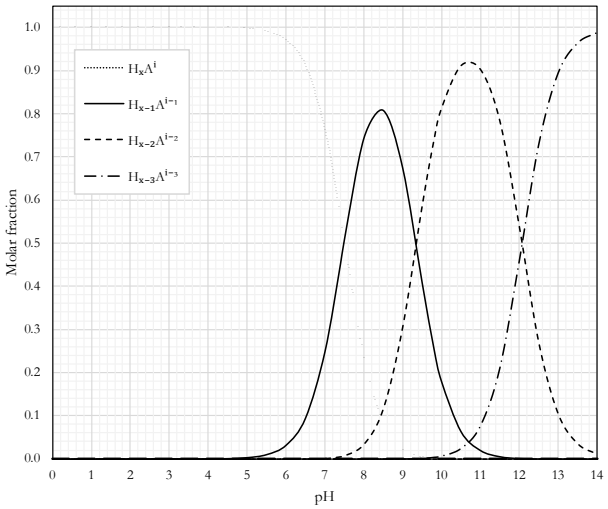

Figure 1. Molar fractions of galangin species plotted as a function of pH.

Relative Reactivity

The ionization potential (IP) and bond dissociation energy (BDE) were systematically computed using the ΔSCF framework to construct the electron and hydrogen-donating ability map for antioxidants, known as eH-DAMA.[55] eH-DAMA visually represents the likelihood of molecules as hydrogen and electron donors, reflecting their capabilities in hydrogen atom transfer and electron transfer mechanisms. The most effective radical scavengers are anticipated to be located in the bottom-left quarter. This approach provides a comprehensive exploration of the molecule's reactivity for comparison purposes.

All undissociated hydroxyl groups within the molecule, potentially acting as hydrogen donors (H•), were considered. The dominant acid-base species of **Glg** at physiological pH, along with two antioxidant references (Trolox and α-tocopherol) and the $H_2O_2/O_2^{\bullet-}$ pair representing the potential oxidant target, were included in this map

The lowest BDE and IP values for the galangin species were estimated as (91.9 kcal mol^{-1}, 5.9 eV) in pentyl ethanoate (**H_3Glg^{PET}**), and (91.3 kcal mol^{-1}, 5.0 eV), (88.0 kcal mol^{-1}, 4.4 eV), (90.6 kcal mol^{-1}, 3.5 eV) for the neutral (**H_3Glg**), monoanionic (**H_2Glg^-**), and dianionic (**$HGlg^{2-}$**) species, respectively. Unfortunately, comparative data in the literature are sparse. In our previous paper[54] employing the B3LYP/6-31+G(d,p)/PCM level of theory, **H_3Glg** was associated with a slightly different BDE value of 86.9 kcal mol^{-1}. However, the IP outputs remained coherent. In another study, Lewandowski et al.[56] reported intrinsic reactivity indices of 78.7 kcal mol^{-1} and 4.83 eV, obtained through computations under the B3LYP/6-311++G(d,p)/PCM regime. The observed inconsistency is not surprising, given B3LYP's known limitations in such studies, in contrast to the level of theory chosen here[57,58]. Furthermore, determining IP is highly reliant on the chosen functional and basis set, emphasizing the need for methodological consistency for accurate and meaningful comparisons in reactivity studies.[58]

Figure 2 illustrates two eH-DAMA maps, one in a nonpolar environment (upper, for pentyl ethanoate) and the other in a polar environment (lower, for water). These maps include reference substances (α-tocopherol, Trolox, ascorbic acid) and various flavonoids (isorhamnethin, scutellarein, apigenin, pinocembrin)[50–53] marked for comparative purposes.

In a nonpolar medium, **H_3Glg^{PET}** shows promise for deactivating free radicals through electron transfer compared to pinocembrin and apigenin. However, based on BDE, all other reductants, except pinocembrin, are projected to undergo hydrogen atom transfer more readily. Notably, the BDE value is on the margin of the box drawn by the $H_2O_2/^{\bullet}OOH$ pair, suggesting that the hydrogen atom transfer process might not be particularly effective

Transitioning to a polar environment, the substance's activity improves significantly, observed in a simultaneous decrease in BDE and IP values. In this environment, any **Glg** species demonstrates the capability to reduce the reference oxidant. Also, consecutive deprotonations significantly impact the IP value. Interestingly, the pattern is similar to that of pinocembrin, but the additional hydroxyl group at C_3 and a double bond between C_2 and C_3 influence the reactivity indices, causing a notable shift towards the zone corresponding to more active antioxidants. While neutral and monoanionic species may not be more effective antiradical agents than Trolox anion and ascorbate, the dianionic form is likely to exhibit an outstanding propensity for electron transfer.

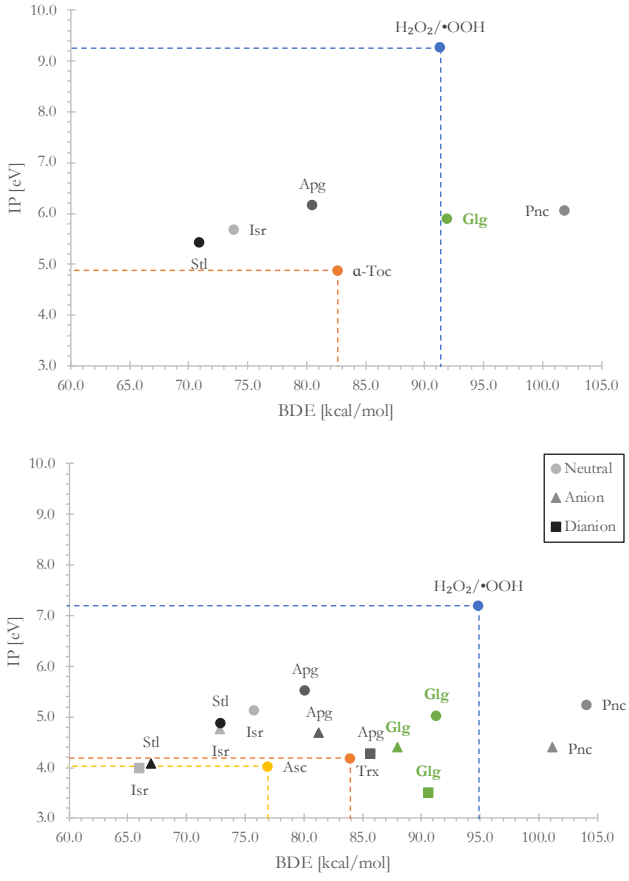

Figure 2. Electron and Hydrogen Donating Ability Maps for Antioxidants including galangin species.

Thermochemistry

Understanding the reaction mechanisms is crucial for rationalizing the reactivity of chemical compounds, particularly in the context of antiradical activity. Three primary pathways govern the antiradical activity of a substance:

- single electron transfer (SET):
$$H_nA^i + R^{\bullet} \rightarrow H_nA^{i+1} + R^{i-1}$$
- formal hydrogen atom transfer (*f*-HAT):
$$H_nA^i + R^{\bullet} \rightarrow H_{n-1}A^i + HR^{\bullet}$$
- radical adduct formation (RAF):
$$H_nA^i + R^{\bullet} \rightarrow [H_nA{-}HR]^{i+\bullet}$$

The evaluation of free radical scavenging activity focuses on the reactions of **Glg** species with the hydroperoxyl radical •OOH. Despite the widely recognized hydroxyl radical, •OH, as the primary initiator of oxidative damage, it high reactivity results in swift rapid reactions with molecules in its proximity before an antioxidant can effectively intercept it. The extended half-lives of peroxyl radicals, including •OOH, offer antioxidants a window of opportunity to successfully intercept them.[2] This characteristic not only aids the in exploring trends in radical scavenging efficiency but also underscores the crucial role of peroxyradicals as essential reaction partners for polyphenolic antioxidants.[59] Additionally, •OOH has been proposed to play a pivotal role in the toxic side effects associated with aerobic respiration.[60]

Figure 3 present the Gibbs free energies (ΔG) for each reaction pathway in lipid and aqueous solutions.

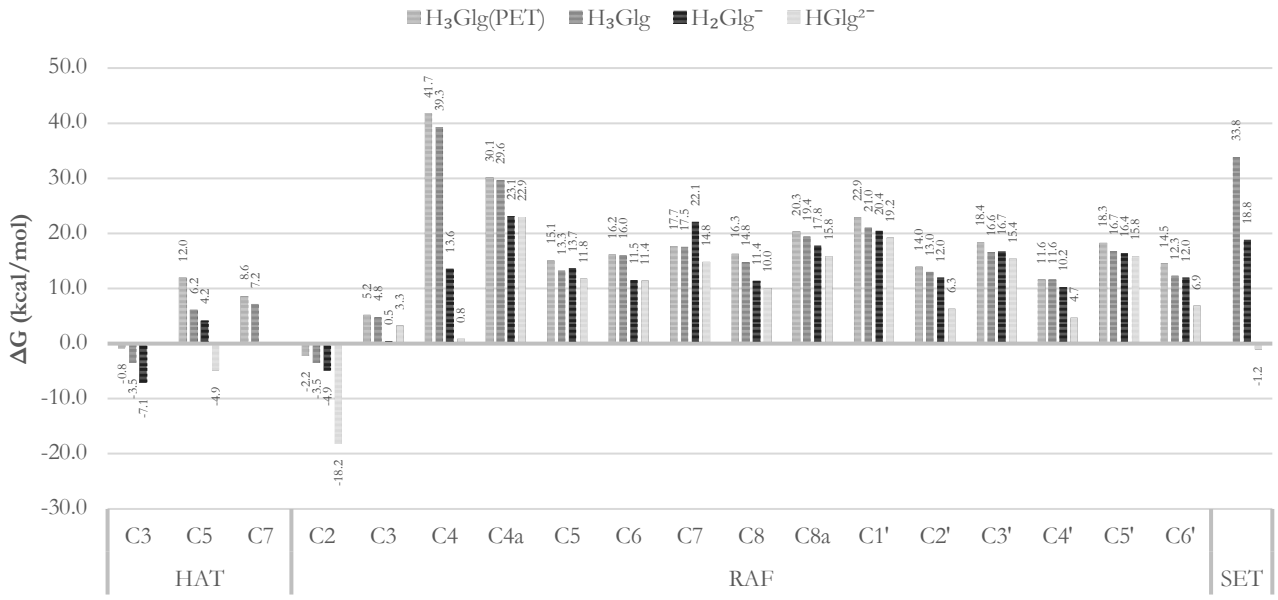

Figure 3. Gibbs free energies of reaction (ΔG, in kcal mol^{-1}, at 298.15 K) for the modeled pathways.

In the lipid solution (**H_3Glg^{PET}**), only two chemical pathways were identified as exergonic: HAT from the phenolic hydroxyl group at C_3 (-0.8 kcal mol^{-1}) and RAF at C_2 (-2.2 kcal mol^{-1}). For **H_3Glg**, both HAT from the C_3 hydroxyl group and RAF at C_2 are equally exergonic, with esteemed values of -3.5 kcal mol^{-1}. As subsequent deprotonation occurs, these values decrease further, reaching -7.1 kcal mol^{-1} for HAT and -4.9 kcal mol^{-1} for RAF in **H_2Glg^-**. In the case of **$HGlg^{2-}$**, which lacks the C_3 hydroxyl group, a ΔG value of -4.9 kcal mol^{-1} is obtained. The pronounced feasibility of hydrogen atom transfer from C_3, compared to other hydrogen-donating sites, can be attributed to the greater degree of delocalisation of the spin density created compared to instances of C_5 or C_7 radicals.[54] Considering the acidic nature of these residues, exergonicity is also somewhat triggered with the polarity of the solvent and subsequent deprotonations.[49]

A particularly unique aspect is the favourable thermochemistry of the radical adduct formation route involving position C_2. The Gibbs free energies remain constantly negative, with an exceptional low value observed for **$HGlg^{2-}$** (-18.2 kcal mol^{-1}), nearly four times lower than for **H_2Glg^-**. This intriguing behaviour is noteworthy, especially when contrasted with the sizably endergonic nature of nearly all other RAF pathways. This suggests that the ability to intercept hydroperoxyl radical could be a subject of debate from the thermochemical standpoint, highlighting the unique and favourable characteristics of the discussed route.

Last but not least, the ΔG values of 33.8 kcal mol^{-1} and 18.8 kcal mol^{-1}, associated with the SET mechanism from **H_3Glg** and **H_2Glg^-** species, respectively, may initially suggest an unfavorable nature of the process. However, caution should be exercised in dismissing these values outright. Electron transfer pathways may play a significant role in overall antiradical activity, potentially surpassing other channels. The efficacy of the mechanism hinges strongly on the established reorganization energies. To systematically explore this relationship, Marcus theory has been applied, calculating activation energies as a function of established reorganization energies and free energies, graphically represented in the Marcus parabola depicted in **Figure 4**.

The obtained high reorganization energies suggest a wide spread of the parabola's arms, indicating substantial structural changes during SET reactions. Additionally, the λ values imply that activation energies change more gradually as ΔG varies, suggesting a less pronounced impact on $\Delta G^{\neq}$ is expected. The parabola's apex is approximately -25.0 kcal mol^{-1}, and all computed ΔG values reside on the descending arm, with the lowest at 6.0 kcal mol^{-1} (**$HGlg^{2-}$**). These findings

support the assertion that **Glg** species likely do not act as electron donors to •OOH, disregarding the potential significance of the SET pathway in overall antiradical activity, except for **HGlg^{2-}**.

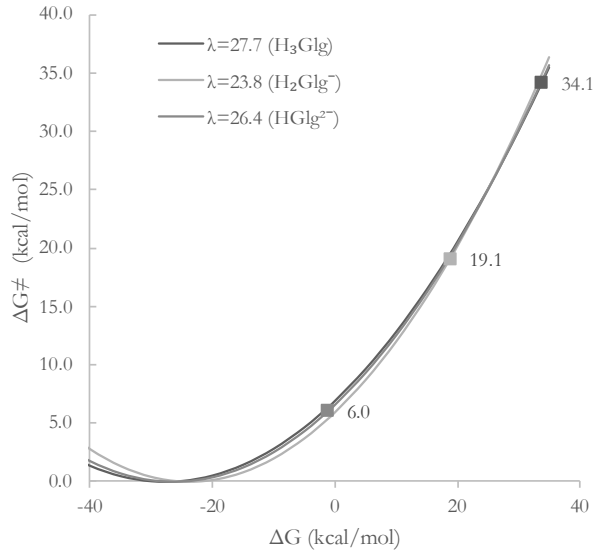

Figure 4. Gibbs free energies of activation (ΔG≠) as a function of Gibbs free energies of reaction (ΔG). λ represents reorganization energies for the given species. The squares correspond to the pair of values. All values are in kcal mol^{-1}, at 298.15 K

Kinetics

Not all pathways identified as endergonic in the previous section were excluded from the kinetic calculations. While it is not expected that the experimentally observed products will result from these reactions, their significance may still be valid. This is especially true if subsequent processes are sufficiently exergonic, providing a driving force, and if the initial step itself is associated with a low activation energy. An example of this scenario can be the formation of radical-ionic species, as they are prone to engage in rapid protonation/deprotonation equilibria. In the complex nature of biological systems with a diverse array of reacting substances, such situations may easily occur in physiological environments.[1,61] Consequently, the kinetic analysis encompasses pathways labelled with positive, albeit low (≤10.0 kcal mol^{-1}), values of ΔG, recognizing their potential relevance in the overall reaction network. In contrast, electron-related processes adhere to Marcus theory, making them all worth investigating..[46,62,63]

Yet, before delving into the kinetic considerations, another crucial aspect must be addressed. The •OOH/$O_2^{\bullet-}$ radical pair exists as part of an acid–base equilibrium with a pK_a of 4.8. In an aqueous solution at pH=7.4, the molar fraction of •OOH is only 0.0025 due to this equilibrium. The superoxide anion radical,, $O_2^{\bullet-}$, functions as a nucleophile and mild reducing agent, exerting minimal impact on biological targets.[64,65] Therefore, its protonated form is considered a primary contributor to oxidative damage, despite its significantly lower molar fraction.[66] Consequently, to accurately replicate data under these conditions, this aspect must be taken into consideration and is hereafter referred to as $k_{•OOH}$.

The exploration of viable mechanisms is elucidated through the determination of rate constants and branching ratios. The pertinent transition state structures are depicted in **Figures 5-8**, accompanied by the corresponding thermochemical data detailed in **Table 4**.

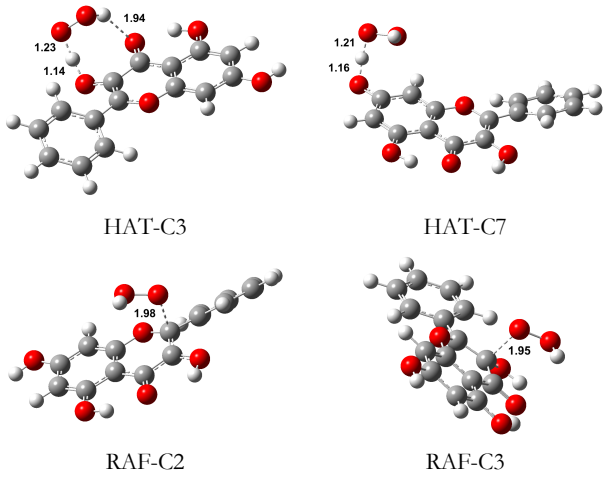

Figure 5. Optimized geometries of the transition states in lipid solution. Distances are reported in angstroms.

The provided kinetic and branching ratios for the reactions in lipid media underscore the significance of the hydrogen atom transfer mechanism. To be more precise, the observed reactivity is predominantly associated with the hydroxyl group at C_3. The notably high rate constant of 3.77 × 10^3 M^{-1} s^{-1} results in a nearly unary branching ratio, emphasizing its prevalence in scavenging the •OOH radical. In contrast, the contribution of the remaining pathways, including HAT from C_7 and RAFs at C_2 and C_3, to the overall activity in lipids is not greater than 0.12%. Thus, at least in this medium, the hydroxyl moiety is identified as responsible for the antioxidant behaviour of the investigated compound.

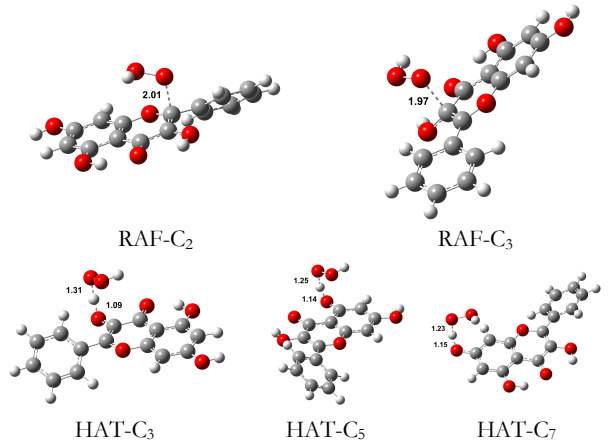

Figure 6. Optimized geometries of the transition states of neutral species in aqueous solution. Distances are reported in angstroms.

In an aqueous solution at physiological pH, the chemistry involved in the peroxyl radical scavenging activity of **Glg** becomes significantly more complex. According to the overall calculated rate constants, **Glg**

is predicted to react with •OOH at a rate of around 1.69×10^5 M^{-1} s^{-1}. This is the sum of individual contributions from **H_3Glg** (6.46×10^3 M^{-1} s^{-1}), **H_2Glg^-** (5.11×10^4) and **$HGlg^{2-}$** (1.31×10^{10}). Nonetheless, while the k_{total} values are generally plausible, with none dropping below 10^3 M^{-1} s^{-1}, the small fraction of •OOH present at this pH (~0.25%) and the varying molar fraction of each species notably interfere with the final outcome.

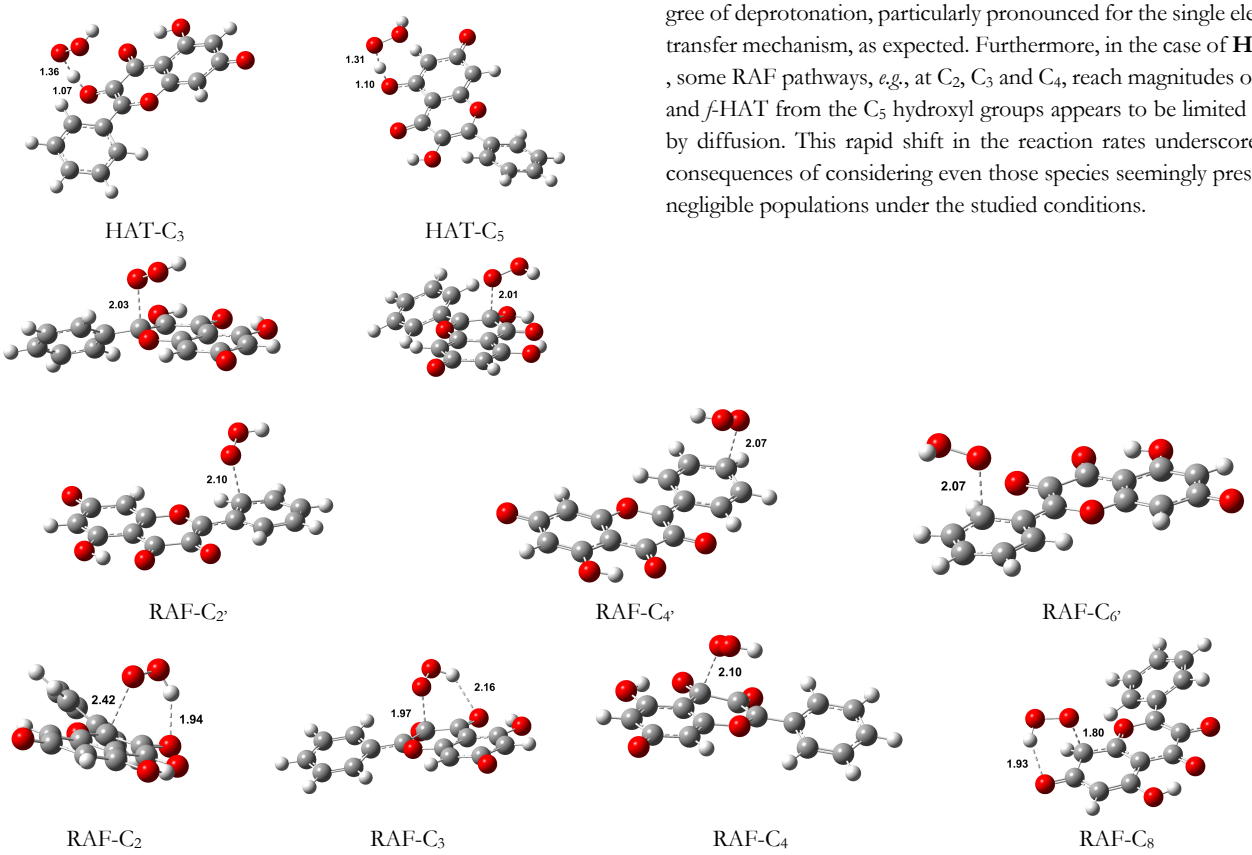

HAT-C_3 HAT-C_5 RAF-$C_{2'}$ RAF-$C_{4'}$ RAF-$C_{6'}$ RAF-C_2 RAF-C_3 RAF-C_4 RAF-C_8

Figure 8. Optimized geometries of the transition states of dianionic species in aqueous solution. Distances are reported in angstrom.

In comparison, when reacting with •OOH, **H_3Glg^{PET}** is approximately 140 times less efficient antioxidant α-tocopherol[67]. However, its capability to scavenge hydroperoxyl radicals in this medium is notably better than apigenin[53] (6500 times greater rate constant) and quite similar to that of scutellarein[51] (around 4 times greater). Shifting to a water solvent, while **Glg** ($k_{overall}$ = 1.69×10^5) is notably less efficient as a scavenger than ascorbate [36] ($k_{overall}$ = 1.00×10^8), it actually outperforms Trolox[68] ($k_{overall}$ = 8.96×10^4). In both media, **Glg** exhibits much better antiradical activity than pinocembrin, other closely related flavonoid.[50]

Table 4. Gibbs free energies of activation ($\Delta G^{\neq}$, kcal mol^{-1}), rate constants (k, M^{-1} s^{-1}) and branching ratios (%) of the reactions between galangin species and hydroperoxyl radical in lipid and aqueous Solution.

	H_3Glg^{PET}			H_3Glg			H_2Glg^-			$HGlg^{2-}$		
	$\Delta G^{\neq}$	k	%	$\Delta G^{\neq}$	k	%	$\Delta G^{\neq}$	k	%	$\Delta G^{\neq}$	k	%
f-HAT												
C_3	16.7	3.77×10^3	99.89	15.4	6.42×10^3	99.30	13.8	5.04×10^4	98.64			
C_5				24.1	1.28×10^{-1}	0.00	22.3	2.88×10^0	0.01	0.0†	8.29×10^9†	63.17
C_7	19.8	1.73×10^0	0.05	22.0	6.95×10^{-1}	0.01						
RAF												
C_2	17.8	8.04×10^{-1}	0.02	15.6	3.33×10^1	0.52	14.2	3.27×10^2	0.64	2.3	2.50×10^9	19.03
C_3	17.3	1.75×10^0	0.05	16.2	1.13×10^1	0.18	14.1	3.64×10^2	0.71	3.5	1.83×10^9	13.97
C_4										5.9	2.74×10^8	2.09
C_8										12.3	6.59×10^3	0.00

RAF-C_2 RAF-C_3

Figure 7. Optimized geometries of the transition states of anionic species in aqueous solution. Distances are reported in angstroms.

The acid−base equilibria of the investigated **Glg** species exert a significant influence on the kinetics of their reactions with peroxyl radicals, thereby impacting their capability as hydroperoxyl radical scavengers. Evidently, the anti-•OOH activity increases with the degree of deprotonation, particularly pronounced for the single electron transfer mechanism, as expected. Furthermore, in the case of **$HGlg^{2-}$**, some RAF pathways, *e.g.*, at C_2, C_3 and C_4, reach magnitudes of 8–9, and *f*-HAT from the C_5 hydroxyl groups appears to be limited solely by diffusion. This rapid shift in the reaction rates underscores the consequences of considering even those species seemingly present in negligible populations under the studied conditions.

$C_{2'}$								15.0	7.11×10^{1}	0.00
$C_{6'}$								14.6	1.42×10^{2}	0.00
SET		34.1	5.89×10^{-13}	0.00	19.1	6.51×10^{-2}	0.00	6.0	2.28×10^{8}	1.74
k_{total}			6.46×10^{3}			5.11×10^{4}			1.31×10^{10}	
$k_{\bullet OOH}$	3.77×10^{3}		8.81×10^{0}			5.78×10^{1}			1.69×10^{5}	
$k_{overall}$						1.69×10^{5}				

† the reaction has been found to be barrierless

Continuing the elucidation on the topic, a comprehensive graph depicting the impact of pH on the overall and species-specific total rate constants is provided (**Figure 9**). It encompasses the pH range of 1.5 to 8.5, corresponding to the acidity found in the stomach and the slight alkalinity present in the small intestine.

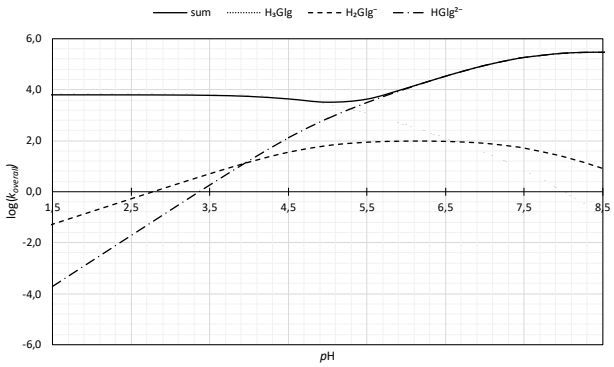

Figure 9. Dependence of kinetics on pH for the reactions between galangin species and hydroperoxyl radicals in aqueous solution.

The observed sum of reaction rates is primarily constituted of two forms — **H_3Glg**, for pH values lower than around 5.0, and **$HGlg^{2-}$** for the remainder. The **H_2Glg^-** appears to be of less significance. Generally, the log($k_{overall}$) value remains stable at the outset in the most acidic environments. Starting from pH~3.5, it slightly drops, and a basin can be clearly observed between the pH values of 4.5 and 6, with the minimum at around 5, associated with log($k_{overall}$) = 3.52. Thereafter, a relatively quick increase in anti-$^{\bullet}$OOH activity is observed, resulting from the growing concentration of **$HGlg^{2-}$** and its particular feasibility to intercept the radical.

Regeneration

Once an antioxidant neutralizes a free radical, it typically loses its scavenging ability. However, in biological systems, antioxidants can be regenerated to their pristine form with the help of other antioxidants like glutathione, vitamin C, or vitamin E. Nonetheless, in an oxidatively stressed environment, their concentrations may be depleted. The superoxide anion radical ($O_2^{\bullet-}$) , which is present in abundance at physiological pH (99.75%), is a strong reductant that might also be capable of mediating the renewal process.

The information presented in **Table 3** illuminates the regeneration dynamics of **Glg** species, offering crucial insights into the energetics and kinetics of their interactions with hydroperoxyl radicals. Remarkably, irrespective of the protonation state and the involved residues, the regeneration process proves to be feasible, as indicated by consistently negative Gibbs free energies. While the viability experiences a gradual decrease with each successive deprotonation step, the process remains favourable, with none of the values reaching an endergonic state. Furthermore, the calculated activation energies, capped at 3.6 kcal mol^{-1} (notably in the cases of C_5 of **$HGlg^{2-}$** and SET from **H_3Glg^-**), suggest rapid reactions limited by diffusion. This implies that, if left unintercepted by the surrounding environmental factors, these reactions could perpetuate a self-sustaining cycle of regeneration and scavenging activity. The significance of this is further underscored by the consistently strongly negative energies of protonation from the solvent for all species, emphasizing the likelihood of successful regeneration and sustained antiradical efficacy.

Table 3. Gibbs free energies of reactions (ΔG, kcal mol^{-1}), Gibbs free energies of activation (ΔG$^{\neq}$, kcal mol^{-1}), rate constants (k, M^{-1} s^{-1}), and Gibbs free energies of protonation (ΔG^{+}, kcal mol^{-1}) at 298.15 K for the regeneration process.

	ΔG	ΔG$^{\neq}$	k	ΔG^{+}
H_3Glg				
C_3	-20.1	1.3	4.00×10^{9}	-32.6
C_5	-29.6	0.8	3.96×10^{9}	-32.8
C_7	-34.2	0.7	3.98×10^{9}	-29.2
SET	-49.2	3.6	3.98×10^{9}	
H_2Glg^-				
C_3	-13.9	0.7	3.45×10^{9}	-35.1
C_5	-21.3	0.1	3.83×10^{9}	-39.1
SET	-34.2	1.0	3.98×10^{9}	
$HGlg^{2-}$				
C_5	-7.5	3.6	3.09×10^{9}	-43.8
SET	-14.2	1.6	3.98×10^{9}	

CONCLUSIONS

This research has provided valuable insights into the acid–base equilibrium and antioxidant behaviour of galangin in physiologically important environments. The determination of pKa values through theoretical estimates, validated by previous studies, revealed a stepwise deprotonation process with distinct preferences for specific hydroxyl groups. The molar fraction analysis highlighted the prevalence of the neutral and first deprotonated forms at physiological pH, simultaneously emphasizing the need to consider even minor populations of charged species.

The eH-DAMA facilitated a comprehensive exploration of **Glg**'s reactivity, particularly in nonpolar and polar environments. The computed IP and BDE values indicated Glg's potential as a radical scavenger, with variations depending on the medium.

Further exploration into reaction mechanisms elucidated the crucial role of the hydroxyl group at C3 in the scavenging activity of **Glg** through hydrogen atom transfer. The kinetic analysis emphasized the predominance of this mechanism in lipid media, showcasing its significant contribution to the overall antioxidant activity. In aqueous

solutions, the complexity of the reactions with hydroperoxyl radicals was evident, with **Glg** demonstrating notable efficiency as a scavenger under physiological conditions.

The study also shed light on the regeneration dynamics of **Glg**, highlighting the feasibility of its renewal after neutralizing free radicals. The calculated activation energies suggested rapid and diffusion-limited reactions, emphasizing the potential for a self-sustaining cycle of regeneration and sustained antiradical efficacy.

In summary, this research not only contributes to the understanding of **Glg**'s acid–base equilibrium and antioxidant behaviour but also underscores the importance of considering environmental factors and reaction pathways in evaluating the overall efficacy of polyphenolic antioxidants in diverse physiological conditions. Further experimental validations and applications of the proposed methodology can enhance our knowledge of these complex systems, offering valuable implications for antioxidant research and drug development.

DATA AND SOFTWARE AVAILABILITY

Gaussian, version G16 (revision C.01), is a proprietary software package copyrighted by Gaussian Inc. (https://gaussian.com). It was accessed through the infrastructure of the Poznan Supercomputing and Networking Center, Wroclaw, Poland.

ASSOCIATED CONTENT

Supporting Information

The Supporting Information is available free of charge on the ACS Publications website.

Cartesian coordinates (PDF)

AUTHOR INFORMATION

Corresponding Author

*E-mail: maciej.spiegel@umw.edu.pl

ORCID

Maciej Spiegel: 0000-0002-8012-1026

ACKNOWLEDGMENT

The research was conducted using the infrastructure of the Poznań Supercomputing and Networking Center**, Wroclaw, Poland.** Marvin was used for drawing, displaying and characterizing chemical structures, Marvin 17.21.0, Chemaxon (https://www.chemaxon.com)

REFERENCE

(1) Sies, H. Oxidative Stress: A Concept in Redox Biology and Medicine. *Redox Biology* **2015**, *4*, 180–183. https://doi.org/10.1016/j.redox.2015.01.002.

(2) Sies, H. Oxidative Stress: Oxidants and Antioxidants. *Experimental Physiology* **1997**, *82* (2), 291–295. https://doi.org/10.1113/expphysiol.1997.sp004024.

(3) Sies, H. Oxidative Stress. In *Stress: Physiology, Biochemistry, and Pathology*; Elsevier, 2019; pp 153–163. https://doi.org/10.1016/B978-0-12-813146-6.00013-8.

(4) Niedzielska, E.; Smaga, I.; Gawlik, M.; Moniczewski, A.; Stankowicz, P.; Pera, J.; Filip, M. Oxidative Stress in Neurodegenerative Diseases. *Mol Neurobiol* **2016**, *53* (6), 4094–4125. https://doi.org/10.1007/s12035-015-9337-5.

(5) Kim, G. H.; Kim, J. E.; Rhie, S. J.; Yoon, S. The Role of Oxidative Stress in Neurodegenerative Diseases. *Experimental Neurobiology* **2015**, *24* (4), 325–340. https://doi.org/10.5607/en.2015.24.4.325.

(6) Sack, M. N.; Fyhrquist, F. Y.; Saijonmaa, O. J.; Fuster, V.; Kovacic, J. C. Basic Biology of Oxidative Stress and the Cardiovascular System. *Journal of the American College of Cardiology* **2017**, *70* (2), 196–211. https://doi.org/10.1016/j.jacc.2017.05.034.

(7) Hayes, J. D.; Dinkova-Kostova, A. T.; Tew, K. D. Oxidative Stress in Cancer. *Cancer Cell* **2020**, *38* (2), 167–197. https://doi.org/10.1016/j.ccell.2020.06.001.

(8) *Antioxidant Vitamins and Trace Elements in Critical Illness - Koekkoek - 2016 - Nutrition in Clinical Practice - Wiley Online Library*. https://aspenjournals.onlinelibrary.wiley.com/doi/abs/10.1177/0884533616653832 (accessed 2024-01-11).

(9) Chiva-Blanch, G.; Visioli, F. Polyphenols and Health: Moving beyond Antioxidants. *Journal of Berry Research* **2012**, *2* (2), 63–71. https://doi.org/10.3233/JBR-2012-028.

(10) Spiegel, M. Current Trends in Computational Quantum Chemistry Studies on Antioxidant Radical Scavenging Activity. *J. Chem. Inf. Model.* **2022**, *62* (11), 2639–2658. https://doi.org/10.1021/acs.jcim.2c00104.

(11) Galano, A.; Mazzone, G.; Alvarez-Diduk, R.; Marino, T.; Alvarez-Idaboy, J. R.; Russo, N. Food Antioxidants: Chemical Insights at the Molecular Level. *Annu. Rev. Food Sci. Technol.* **2016**, *7* (1), 335–352. https://doi.org/10.1146/annurev-food-041715-033206.

(12) Pisoschi, A. M.; Pop, A.; Iordache, F.; Stanca, L.; Predoi, G.; Serban, A. I. Oxidative Stress Mitigation by Antioxidants - An Overview on Their Chemistry and Influences on Health Status. *European Journal of Medicinal Chemistry* **2021**, *209*, 112891. https://doi.org/10.1016/j.ejmech.2020.112891.

(13) Patel, D. K.; Patel, K.; Gadewar, M.; Tahilyani, V. Pharmacological and Bioanalytical Aspects of Galangin-a Concise Report. *Asian Pacific Journal of Tropical Biomedicine* **2012**, *2* (1, Supplement), S449–S455. https://doi.org/10.1016/S2221-1691(12)60205-6.

(14) Sangaraju, R.; Alavala, S.; Nalban, N.; Jerald, M. K.; Sistla, R. Galangin Ameliorates Imiquimod-Induced Psoriasis-like Skin Inflammation in BALB/c Mice via down Regulating NF-κB and Activation of Nrf2 Signaling Pathways. *International Immunopharmacology* **2021**, *96*, 107754. https://doi.org/10.1016/j.intimp.2021.107754.

(15) Thapa, R.; Afzal, O.; Alfawaz Altamimi, A. S.; Goyal, A.; Almalki, W. H.; Alzarea, S. I.; Kazmi, I.; Jakhmola, V.; Singh, S. K.; Dua, K.; Gilhotra, R.; Gupta, G. Galangin as an Inflammatory Response Modulator: An Updated Overview and Therapeutic Potential. *Chemico-Biological Interactions* **2023**, *378*, 110482. https://doi.org/10.1016/j.cbi.2023.110482.

(16) Abukhalil, M. H.; Althunibat, O. Y.; Aladaileh, S. H.; Al-Amarat, W.; Obeidat, H. M.; Al-khawalde, A. A. A.; Hussein, O. E.; Alfwuaires, M. A.; Algefare, A. I.; Alanazi, K. M.; Al-Swailmi, F. K.; Arab, H. H.; Mahmoud, A. M. Galangin Attenuates Diabetic Cardiomyopathy through Modulating Oxidative Stress, Inflammation and

Apoptosis in Rats. *Biomedicine & Pharmacotherapy* **2021**, *138*, 111410. https://doi.org/10.1016/j.biopha.2021.111410.

(17) Salama, S. A.; Elshafey, M. M. Galangin Mitigates Iron Overload-Triggered Liver Injury: Up-Regulation of PPARγ and Nrf2 Signaling, and Abrogation of the Inflammatory Responses. *Life Sciences* **2021**, *283*, 119856. https://doi.org/10.1016/j.lfs.2021.119856.

(18) Galano, A.; Raúl Alvarez-Idaboy, J. Computational Strategies for Predicting Free Radical Scavengers' Protection against Oxidative Stress: Where Are We and What Might Follow? *Int J of Quantum Chemistry* **2019**, *119* (2), e25665. https://doi.org/10.1002/qua.25665.

(19) Spiegel, M.; Marino, T.; Prejanò, M.; Russo, N. Antioxidant and Copper-Chelating Power of New Molecules Suggested as Multiple Target Agents against Alzheimer's Disease. A Theoretical Comparative Study. *Phys. Chem. Chem. Phys.* **2022**, *24* (26), 16353–16359. https://doi.org/10.1039/D2CP01918C.

(20) Pérez-González, A.; Castañeda-Arriaga, R.; Guzmán-López, E. G.; Hernández-Ayala, L. F.; Galano, A. Chalcone Derivatives with a High Potential as Multifunctional Antioxidant Neuroprotectors. *ACS Omega* **2022**, *7* (43), 38254–38268. https://doi.org/10.1021/acsomega.2c05518.

(21) Castro-González, L. M.; Alvarez-Idaboy, J. R.; Galano, A. Computationally Designed Sesamol Derivatives Proposed as Potent Antioxidants. *ACS Omega* **2020**, *5* (16), 9566–9575. https://doi.org/10.1021/acsomega.0c00898.

(22) Pracht, P.; Bohle, F.; Grimme, S. Automated Exploration of the Low-Energy Chemical Space with Fast Quantum Chemical Methods. *Phys. Chem. Chem. Phys.* **2020**, *22* (14), 7169–7192. https://doi.org/10.1039/C9CP06869D.

(23) Frisch, M. J.; Trucks, G. W.; Schlegel, H. B.; Scuseria, G. E.; Robb, M. A.; Cheeseman, J. R.; Scalmani, G.; Barone, V.; Petersson, G. A.; Nakatsuji, H.; Li, X.; Caricato, M.; Marenich, A. V.; Bloino, J.; Janesko, B. G.; Gomperts, R.; Mennucci, B.; Hratchian, H. P.; Ortiz, J. V.; Izmaylov, A. F.; Sonnenberg, J. L.; Williams-Young, D.; Ding, F.; Lipparini, F.; Egidi, F.; Goings, J.; Peng, B.; Petrone, A.; Henderson, T.; Ranasinghe, D.; Zakrzewski, V. G.; Gao, J.; Rega, N.; Zheng, G.; Liang, W.; Hada, M.; Ehara, M.; Toyota, K.; Fukuda, R.; Hasegawa, J.; Ishida, M.; Nakajima, T.; Honda, Y.; Kitao, O.; Nakai, H.; Vreven, T.; Throssell, K.; Montgomery, J. A., Jr.; Peralta, J. E.; Ogliaro, F.; Bearpark, M. J.; Heyd, J. J.; Brothers, E. N.; Kudin, K. N.; Staroverov, V. N.; Keith, T. A.; Kobayashi, R.; Normand, J.; Raghavachari, K.; Rendell, A. P.; Burant, J. C.; Iyengar, S. S.; Tomasi, J.; Cossi, M.; Millam, J. M.; Klene, M.; Adamo, C.; Cammi, R.; Ochterski, J. W.; Martin, R. L.; Morokuma, K.; Farkas, O.; Foresman, J. B.; Fox, D. J. Gaussian˜16 Revision C.01, 2016.

(24) Zhao, Y.; Schultz, N. E.; Truhlar, D. G. Design of Density Functionals by Combining the Method of Constraint Satisfaction with Parametrization for Thermochemistry, Thermochemical Kinetics, and Noncovalent Interactions. *J. Chem. Theory Comput.* **2006**, *2* (2), 364–382. https://doi.org/10.1021/ct0502763.

(25) Zhao, Y.; Truhlar, D. G. How Well Can New-Generation Density Functionals Describe the Energetics of Bond-Dissociation Reactions Producing Radicals? *J. Phys. Chem. A* **2008**, *112* (6), 1095–1099. https://doi.org/10.1021/jp7109127.

(26) Galano, A.; Alvarez-Idaboy, J. R. Kinetics of Radical-molecule Reactions in Aqueous Solution: A Benchmark Study of the Performance of Density Functional Methods. *J Comput Chem* **2014**, *35* (28), 2019–2026. https://doi.org/10.1002/jcc.23715.

(27) Marenich, A. V.; Cramer, C. J.; Truhlar, D. G. Universal Solvation Model Based on Solute Electron Density and on a Continuum Model of the Solvent Defined by the Bulk Dielectric Constant and Atomic Surface Tensions. *J. Phys. Chem. B* **2009**, *113* (18), 6378–6396. https://doi.org/10.1021/jp810292n.

(28) Haynes, W. M. *CRC Handbook of Chemistry and Physics*; CRC Press, 2016.

(29) Ribeiro, R. F.; Marenich, A. V.; Cramer, C. J.; Truhlar, D. G. Use of Solution-Phase Vibrational Frequencies in Continuum Models for the Free Energy of Solvation. *J. Phys. Chem. B* **2011**, *115* (49), 14556–14562. https://doi.org/10.1021/jp205508z.

(30) Fukui, K. The Path of Chemical Reactions - the IRC Approach. *Acc. Chem. Res.* **1981**, *14* (12), 363–368. https://doi.org/10.1021/ar00072a001.

(31) Fukui, K. Formulation of the Reaction Coordinate. *J. Phys. Chem.* **1970**, *74* (23), 4161–4163. https://doi.org/10.1021/j100717a029.

(32) Galano, A.; Pérez-González, A.; Castañeda-Arriaga, R.; Muñoz-Rugeles, L.; Mendoza-Sarmiento, G.; Romero-Silva, A.; Ibarra-Escutia, A.; Rebollar-Zepeda, A. M.; León-Carmona, J. R.; Hernández-Olivares, M. A.; Alvarez-Idaboy, J. R. Empirically Fitted Parameters for Calculating p K_a Values with Small Deviations from Experiments Using a Simple Computational Strategy. *J. Chem. Inf. Model.* **2016**, *56* (9), 1714–1724. https://doi.org/10.1021/acs.jcim.6b00310.

(33) Marković, Z.; Tošović, J.; Milenković, D.; Marković, S. Revisiting the Solvation Enthalpies and Free Energies of the Proton and Electron in Various Solvents. *Computational and Theoretical Chemistry* **2016**, *1077*, 11–17. https://doi.org/10.1016/j.comptc.2015.09.007.

(34) Okuno, Y. Theoretical Investigation of the Mechanism of the Baeyer-Villiger Reaction in Nonpolar Solvents. *Chemistry A European J* **1997**, *3* (2), 212–218. https://doi.org/10.1002/chem.19970030208.

(35) Benson, S. W. *The Foundations of Chemical Kinetics*; Advanced Chemistry Series; McGraw-Hill, 1960.

(36) Galano, A.; Alvarez-Idaboy, J. R. A Computational Methodology for Accurate Predictions of Rate Constants in Solution: Application to the Assessment of Primary Antioxidant Activity. *J Comput Chem* **2013**, *34* (28), 2430–2445. https://doi.org/10.1002/jcc.23409.

(37) Evans, M. G.; Polanyi, M. Some Applications of the Transition State Method to the Calculation of Reaction Velocities, Especially in Solution. *Trans. Faraday Soc.* **1935**, *31*, 875. https://doi.org/10.1039/tf9353100875.

(38) Truhlar, D. G.; Garrett, B. C.; Klippenstein, S. J. Current Status of Transition-State Theory. *J. Phys. Chem.* **1996**, *100* (31), 12771–12800. https://doi.org/10.1021/jp953748q.

(39) Eyring, H. The Activated Complex in Chemical Reactions. *The Journal of Chemical Physics* **1935**, *3* (2), 107–115. https://doi.org/10.1063/1.1749604.

(40) Eckart, C. The Penetration of a Potential Barrier by Electrons. *Phys. Rev.* **1930**, *35* (11), 1303–1309. https://doi.org/10.1103/PhysRev.35.1303.

(41) Pollak, E.; Pechukas, P. Symmetry Numbers, Not Statistical Factors, Should Be Used in Absolute Rate Theory and in Broensted Relations. *J. Am. Chem. Soc.* **1978**, *100* (10), 2984–2991. https://doi.org/10.1021/ja00478a009.

(42) Laidler, K. J. *Chemical Kinetics*, 3. ed., [Nachdr.].; HarperCollins New York, N.Y.: New York, N.Y., 1998.

(43) Kuppermann, A.; Truhlar, D. G. Exact Tunneling Calculations. *J. Am. Chem. Soc.* **1971**, *93* (8), 1840–1851. https://doi.org/10.1021/ja00737a002.

(44) Truhlar, D. G.; Hase, W. L.; Hynes, J. T. Current Status of Transition-State Theory. *J. Phys. Chem.* **1983**, *87* (15), 2664–2682. https://doi.org/10.1021/j100238a003.

(45) Marcus, R. A. Electron Transfer Reactions in Chemistry. Theory and Experiment. *Rev. Mod. Phys.* **1993**, *65* (3), 599–610. https://doi.org/10.1103/RevModPhys.65.599.

(46) Marcus, R. A.; Sutin, N. Electron Transfers in Chemistry and Biology. *Biochimica et Biophysica Acta (BBA) - Reviews on Bioenergetics* **1985**, *811* (3), 265–322. https://doi.org/10.1016/0304-4173(85)90014-X.

(47) Collins, F. C.; Kimball, G. E. Diffusion-Controlled Reaction Rates. *Journal of Colloid Science* **1949**, *4* (4), 425–437. https://doi.org/10.1016/0095-8522(49)90023-9.

(48) Smoluchowski, M. V. Versuch Einer Mathematischen Theorie Der Koagulationskinetik Kolloider Lösungen. *Zeitschrift für Physikalische Chemie* **1918**, *92U* (1), 129–168. https://doi.org/10.1515/zpch-1918-9209.

(49) Spiegel, M.; Cel, K.; Sroka, Z. The Mechanistic Insights into the Role of pH and Solvent on Antiradical and Prooxidant Properties of Polyphenols — Nine Compounds Case Study. *Food Chemistry* **2023**, *407*, 134677. https://doi.org/10.1016/j.foodchem.2022.134677.

(50) Spiegel, M. Theoretical Insights into the Oxidative Stress-Relieving Properties of Pinocembrin─An Isolated Flavonoid from Honey and Propolis. *J. Phys. Chem. B* **2023**, *127* (41), 8769–8779. https://doi.org/10.1021/acs.jpcb.3c03545.

(51) Spiegel, M.; Marino, T.; Prejanò, M.; Russo, N. On the Scavenging Ability of Scutellarein against the OOH Radical in Water and Lipid-like Environments: A Theoretical Study. *Antioxidants* **2022**, *11* (2), 224. https://doi.org/10.3390/antiox11020224.

(52) Spiegel, M.; Ciardullo, G.; Marino, T.; Russo, N. Computational Investigation on the Antioxidant Activities and on the Mpro SARS-CoV-2 Non-Covalent Inhibition of Isorhamnetin. *Front. Chem.* **2023**, *11*, 1122880. https://doi.org/10.3389/fchem.2023.1122880.

(53) Spiegel, M.; Sroka, Z. Quantum-Mechanical Characteristics of Apigenin: Antiradical, Metal Chelation and Inhibitory Properties in Physiologically Relevant Media. *Fitoterapia* **2023**, *164* (October 2022), 105352. https://doi.org/10.1016/j.fitote.2022.105352.

(54) Spiegel, M.; Andruniów, T.; Sroka, Z. Flavones' and Flavonols' Antiradical Structure–Activity Relationship—A Quantum Chemical Study. *Antioxidants* **2020**, *9* (6), 461. https://doi.org/10.3390/antiox9060461.

(55) Guzman-Lopez, E.; Reina, M.; Perez-Gonzalez, A.; Francisco-Marquez, M.; Hernandez-Ayala, L.; Castañeda-Arriaga, R.; Galano, A. CADMA-Chem: A Computational Protocol Based on Chemical Properties Aimed to Design Multifunctional Antioxidants. *IJMS* **2022**, *23* (21), 13246. https://doi.org/10.3390/ijms232113246.

(56) Lewandowski, W.; Lewandowska, H.; Golonko, A.; Świderski, G.; Świsłocka, R.; Kalinowska, M. Correlations between Molecular Structure and Biological Activity in "Logical Series" of Dietary Chromone Derivatives. *PLoS ONE* **2020**, *15* (8), e0229477. https://doi.org/10.1371/journal.pone.0229477.

(57) De Souza, G. L. C.; Peterson, K. A. Benchmarking Antioxidant-Related Properties for Gallic Acid through the Use of DFT, MP2, CCSD, and CCSD(T) Approaches. *J. Phys. Chem. A* **2021**, *125* (1), 198–208. https://doi.org/10.1021/acs.jpca.0c09116.

(58) Spiegel, M.; Gamian, A.; Sroka, Z. A Statistically Supported Antioxidant Activity DFT Benchmark—The Effects of Hartree–Fock Exchange and Basis Set Selection on Accuracy and Resources Uptake. *Molecules* **2021**, *26* (16), 5058. https://doi.org/10.3390/molecules26165058.

(59) Rose, R. C.; Bode, A. M. Biology of Free Radical Scavengers: An Evaluation of Ascorbate. *FASEB j.* **1993**, *7* (12), 1135–1142. https://doi.org/10.1096/fasebj.7.12.8375611.

(60) De Grey, A. D. N. J. $HO_2^{\bullet}$: The Forgotten Radical. *DNA and Cell Biology* **2002**, *21* (4), 251–257. https://doi.org/10.1089/104454902753759672.

(61) Banani, S. F.; Lee, H. O.; Hyman, A. A.; Rosen, M. K. Biomolecular Condensates: Organizers of Cellular Biochemistry. *Nat Rev Mol Cell Biol* **2017**, *18* (5), 285–298. https://doi.org/10.1038/nrm.2017.7.

(62) Marcus, R. A. Chemical and Electrochemical Electron-Transfer Theory. *Annu. Rev. Phys. Chem.* **1964**, *15* (1), 155–196. https://doi.org/10.1146/annurev.pc.15.100164.001103.

(63) Marcus, R. A. On the Theory of Oxidation-Reduction Reactions Involving Electron Transfer. II. Applications to Data on the Rates of Isotopic Exchange Reactions. *The Journal of Chemical Physics* **1957**, *26* (4), 867–871. https://doi.org/10.1063/1.1743423.

(64) Fridovich, I. SUPEROXIDE RADICAL AND SUPEROXIDE DISMUTASES. *Annu. Rev. Biochem.* **1995**, *64* (1), 97–112. https://doi.org/10.1146/annurev.bi.64.070195.000525.

(65) Fridovich, I. Superoxide Radical: An Endogenous Toxicant. *Annu. Rev. Pharmacol. Toxicol.* **1983**, *23* (1), 239–257. https://doi.org/10.1146/annurev.pa.23.040183.001323.

(66) Bielski, B. H. J.; Cabelli, D. E.; Arudi, R. L.; Ross, A. B. Reactivity of HO2/O−2 Radicals in Aqueous Solution. *Journal of Physical and Chemical Reference Data* **1985**, *14* (4), 1041–1100. https://doi.org/10.1063/1.555739.

(67) Navarrete, M.; Rangel, C.; Espinosa-García, J.; Corchado, J. C. Theoretical Study of the Antioxidant Activity of Vitamin E: Reactions of α-Tocopherol with the Hydroperoxy Radical. *J. Chem. Theory Comput.* **2005**, *1* (2), 337–344. https://doi.org/10.1021/ct0498932.

(68) Alberto, M. E.; Russo, N.; Grand, A.; Galano, A. A Physicochemical Examination of the Free Radical Scavenging Activity of Trolox: Mechanism, Kinetics and Influence of the Environment. *Phys. Chem. Chem. Phys.* **2013**, *15* (13), 4642. https://doi.org/10.1039/c3cp43319f.

TABLE OF CONTENTS GRAPHIC